3.5

MACHINE INTELLIGENT GUST FRONT ALGORITHM FOR THE TERMINAL DOPPLER WEATHER RADAR (TDWR) AND INTEGRATED TERMINAL WEATHER SYSTEM (ITWS)*‡

Seth W. Troxel, Richard L. Delanoy, John P. Morgan, and William L. Pughe†

MIT Lincoln Laboratory
Lexington, Massachusetts

1. INTRODUCTION

Thunderstorms often generate gust fronts that can have significant impact on airport operations. Unanticipated changes in wind speed and direction are of concern from an air traffic safety viewpoint (hazardous wind shear) as well as from an airport planning point of view (runway configuration). Automated gust front detection is viewed by FAA and the air traffic community as an important component of current and future hazardous weather detection systems including the Terminal Doppler Weather Radar (TDWR), ASR–9 with Weather Systems Processor (ASR–9 WSP), and the Integrated Terminal Weather System (ITWS) for which TDWR is a principal sensor.

In cooperation with the FAA, Lincoln Laboratory has successfully developed and tested a real–time Machine Intelligent Gust Front Algorithm (MIGFA) for use with Doppler weather radars. This algorithm resulted from the successful fusion of two complementing technologies developed at Lincoln Laboratory: computer vision/machine intelligence techniques originally developed for automated target recognition, and automated product–oriented weather radar data processing. Using these techniques, a version of MIGFA designed for use with TDWR has demonstrated substantial improvement over the existing TDWR gust front algorithm, detecting more and greater extents of gust fronts with fewer false alarms. MIGFA is slated to eventually replace the existing TDWR gust front algorithm and will be used as the gust front algorithm for the planned ITWS and ASR–9 WSP systems.

A brief overview of techniques used by MIGFA to identify and track gust fronts will be presented in this paper. More details, along with recent detection performance results, can be obtained from prior publications [Verly, 1989; Troxel, 1994; Lincoln Laboratory, 1995]. However, detection and tracking of a gust front is only part of the task. Once the location of a gust front has been determined, the associated wind shear estimate and wind shift forecast must be computed. Several issues arise. For example, a gust front can be tens of kilometers in length, with outflow strength and contrasting environmental winds varying considerably along its length. Where along the front should the wind shear analysis be performed? Also, for airport planning purposes, air traffic controllers and managers need to plan runway configuration based on winds that may change suddenly when a gust front moves over the airport. Depending on the nature of the gust front, some of these wind shifts are relatively transient while others are more persistent. How should the wind shift advisory produced by the algorithm take this into account?

MIGFA uses a consensus derived from a variety of estimation techniques as a robust means of generating wind shear and wind shift estimates for detected gust fronts. These techniques, and some of their limitations, are discussed. Results of comparisons of MIGFA–generated wind shear and wind shift reports against observations are also presented. The paper concludes by outlining planned enhancements to incorporate additional information available under ITWS that should further improve the quality of MIGFA's wind shear and wind shift forecasts.

2. ALGORITHM DESIGN

2.1. Overview

The system block diagram in Figure 1 illustrates the current configuration of MIGFA as designed for TDWR/ITWS. The design is nearly identical to the ASR–9 WSP version except for the types of feature detectors employed. In preparation for processing, input TDWR base data images DZ (reflectivity) and V (Doppler velocity) are converted from polar (400 range bins X 360 radials) to Cartesian (260 X 260) representations with 500 m pixel resolution. A map of radial shear representing the radial velocity change over a 1 km distance is computed from linear regression of Doppler velocities within successive 1–km windows, and serves as a third input image called DV. The input images are then passed to multiple simple independent feature detectors (more detail on these to follow) that attempt to localize those features that are selectively indicative of gust fronts. The outputs of each of these feature detectors, most of which are based on some application of functional template correlation (FTC) [Delanoy, 1992], are expressed as interest images that specify evidence indicating where and with what confidence a gust front may be present. The different interest images are fused to form a combined interest image, providing an overall map of evidence indicating the locations of possible gust fronts.

From the combined interest image, fronts are extracted as chains of points. The chains extracted from a radar scan, collectively called an event, are integrated with prior events by establishing a point–to–point correspondence. Heuristics are then ap-

*This work was sponsored by the Federal Aviation Administration. The views expressed are those of the authors and do not reflect the official policy or position of the U.S Government.

‡Opinions, interpretations, conclusions, and recommendations are those of the authors and are not necessarily endorsed by the United States Air Force.

†*Corresponding author address:* Seth W. Troxel, MIT Lincoln Laboratory, 244 Wood Street, Lexington, MA 02173–9108; e–mail <setht@ll.mit.edu>

plied to reject those chain points which have an apparent motion that is improbable and to edit properties of individual points that are inconsistent with their neighbors. For each resulting chain, a wind shift estimate and a wind shear hazard estimate is then computed using a variety of wind analysis methods operating on appropriate regions of the the input Doppler velocity imagery and, where available and appropriate, utilizing additional sources of wind information such as anemometer data (e.g., airport LLWAS centerfield wind reports). Following wind analysis, the newly updated gust front history is used to make flexible, point–by–point predictions of where points along the front will be located as some future time. Such predictions are also used in the processing of subsequent images, specifically in the feature detector called ANTICIPATION (described later).

2.2. Feature Detectors

TDWR base reflectivity and Doppler velocity data are processed by MIGFA using approximately ten different FTC–based feature detectors. Figure 2 shows several interest images produced by applications of FTC to the input images that are displayed in gray–scale along the top row of the figure (in the velocity image V, white pixels indicate strong winds directed away from the radar, while black pixels indicate strong winds directed toward the radar). The figure also shows the combined interest image resulting from combination of the individual interest images. Homogenous, mid–level gray regions denote mask areas where specific feature detectors are prevented from expressing an opinion regarding the presence of a gust front, deferring instead to the evidence generated by other feature detectors. In each of the interest images, white pixels indicate locations of maximum confirming interest, while black pixels indicate locations of maximum disconfirming or negative interest.

The first interest image in the second row (TDWR–TL–DZ–CONV) is generated by a tandem feature detector that looks for thin lines in the DZ image that are coincident and aligned with velocity convergence in the DV image. Since obscuration prevents detection of thin line echoes inside storm cells, the TDWR–TL–DZ–CONV detector is prevented from generating opinions in these areas.

The TDWR–DZ–CONV–MOTION detector is similar to TDWR–TL–DZ–CONV except that it looks for tandem motion of reflectivity thin lines and velocity convergence lines. Motion detectors are based on simple differencing. The DZ image from the previous scan (received approximately 5 minutes earlier) is subtracted from the DZ image from the current scan. In the differenced DZ image, gust fronts appear as white lines (positive values at the front's position in the current scan) that are trailed by parallel dark lines (negative values at the front's position in the previous scan). The functional template returns maximal scores where thin lines of positive values occur.

The interest image labelled TDWR–ASSORTED–MOTION represents the combined (maximum) evidence from a number of single feature detectors. This constitutes a comparatively liberal detector that helps to offset the relatively conservative opinions produced by the tandem detectors.

The TDWR–CELL–CONVERGE detector looks for velocity convergence boundaries specifically within storm regions. Note that in this detector, all non–storm regions have been masked so that the detector is prevented from expressing an opinion outside of storm regions.

The TDWR–HIGH–CONVERGE detector is designed to provide additional interest wherever there are very strong velocity convergence boundaries. This detector is an important element in that it helps to ensure detection of potentially hazardous wind shears when there might not otherwise be enough supporting evidence from other detectors.

Finally, the ANTICIPATION feature detector provides a mechanism for spatially adjusting the detection sensitivity of MIGFA on the basis of knowledge of various environmental data including the prior history of the gust fronts being tracked and dominant weather patterns. Anticipation works by creating bands of high interest values where the object is expected to be in the current scan. Anticipation is set not so high as to trigger a detection by itself (i.e., coasting), but high enough to raise collocated weak signals above detection threshold.

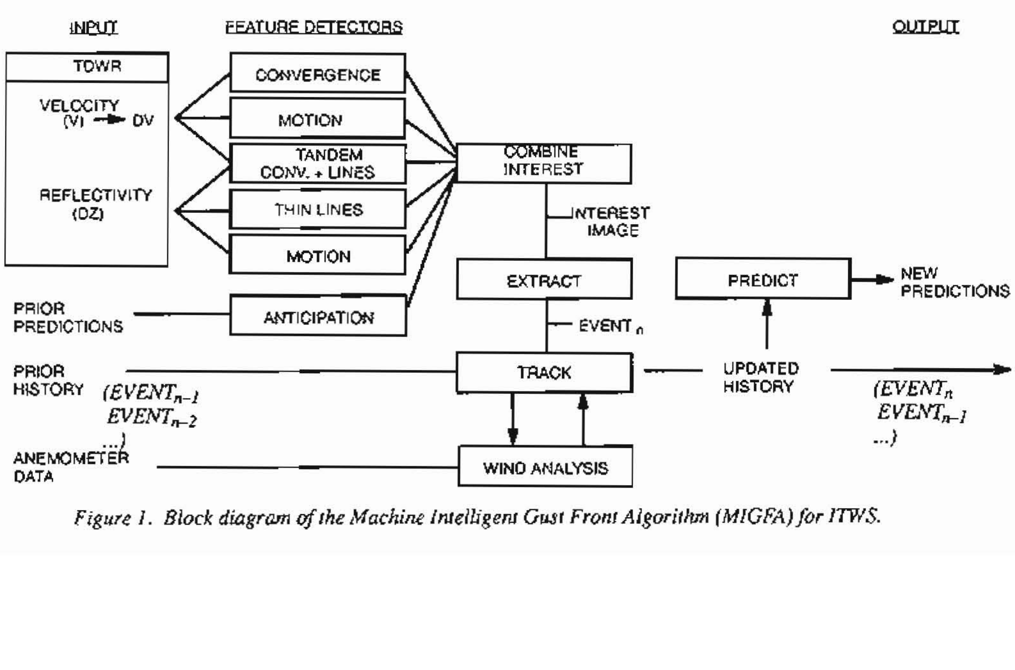

Figure 1. Block diagram of the Machine Intelligent Gust Front Algorithm (MIGFA) for ITWS.

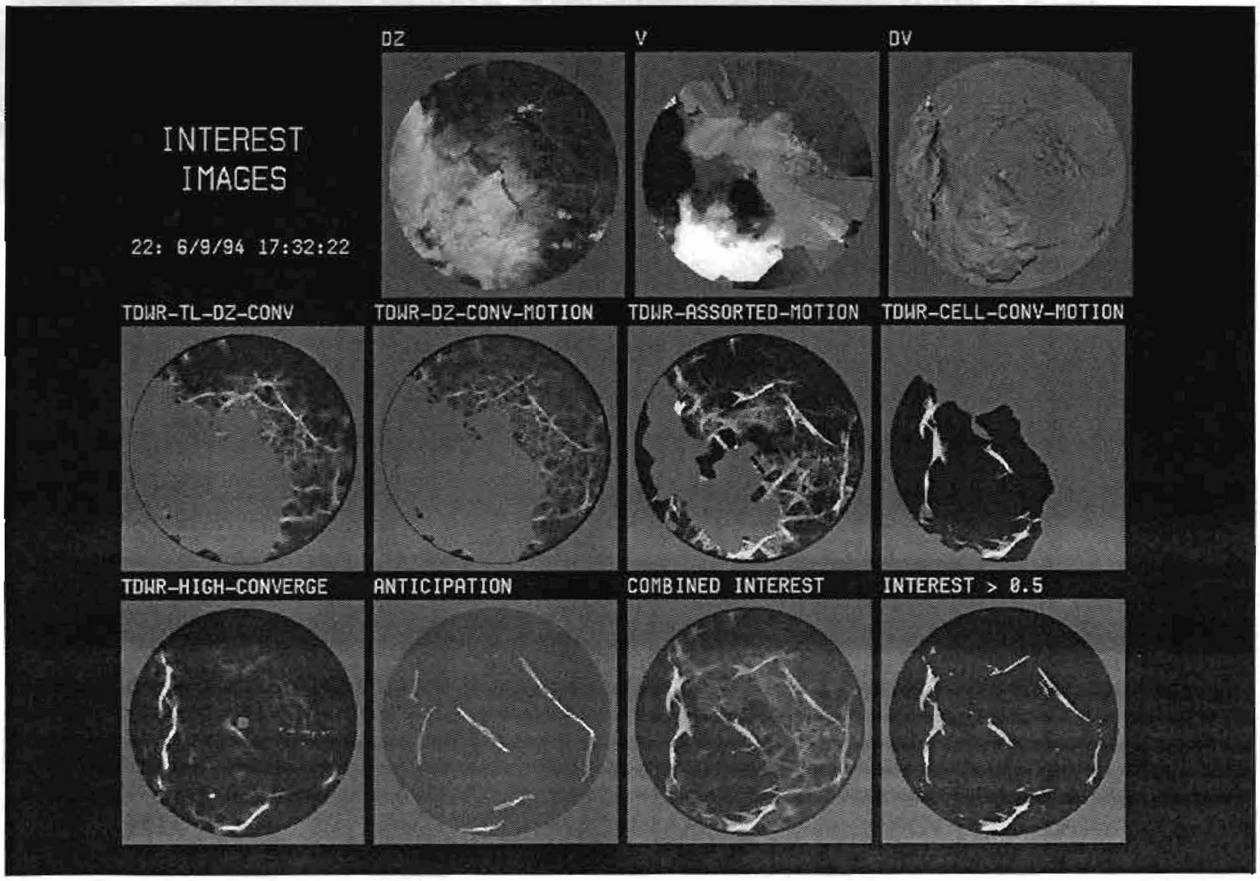

Figure 2. Combining of interest images. Input DZ (reflectivity), V (velocity), and DV (velocity change) images are shown along with output interest images from some of the feature detectors. The last two frames in the lower right show the images resulting from combining the various interest images.

3. WINDFIELD ANALYSIS

In order to generate wind shift forecasts and wind shear hazard reports, wind field analyses need to be conducted on different spatial scales and at different locations about the front. For runway planning purposes, wind shift forecasts are operationally useful when they indicate what the persistent winds are at some distance behind the front, while meaningful wind shear hazard estimates require an analysis that captures the velocity gradient across the frontal zone. We found that using a single estimation technique worked well for many cases, but produced less than satisfactory results given various combinations of viewing geometry and data quality problems.

Instead of using a single wind estimation method, MIGFA utilizes a multi–algorithmic consensus approach. Several different techniques of Doppler wind field analyses are performed in regions behind, ahead, and inside of a selected segment of the gust front as show in Figure 3. Additional wind estimates are obtained from airport anemometer data (Figure 4). The various localized wind analyses are used in construction of the wind shift forecasts and wind shear hazard reports.

First, a segment of the gust front over which the wind analysis will be performed is chosen based on the distance of the front from the airport reference point (ARP). As long as a detected front together with its 20–minute position forecast lie outside an airport control radius parameter (nominally 15 km), MIGFA simply chooses a 12 km segment centered about the front's midpoint as the focal point for the wind analysis. However, once the nearest point of a gust front moves to within 20 minutes of the airport control radius, the analysis region is shifted to correspond to the 12–km segment of the front that is forecasted to pass over the airport. This localization of the wind analysis is important because gust fronts can extend for tens of kilometers and can have outflow strengths that vary considerably along their lengths. Once the appropriate gust front segment has been identified, multiple wind field analyses are conducted within the three analysis regions shown in Figure 3. For each analysis region and where appropriate, wind estimates are obtained using the following techniques:

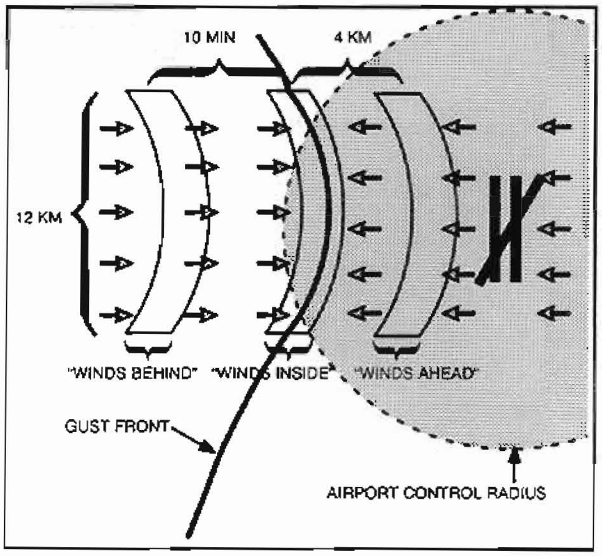

Figure 3. Doppler wind analysis regions for MIGFA wind shift and wind shear estimation.

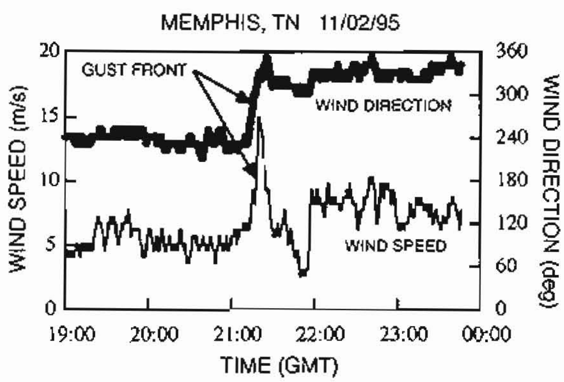

Figure 4. Gust front passage at Memphis Int'l Airport (circa 21:15 GMT) revealed in airport LLWAS centerfield anemometer data.

1. **Perpendicular wind model.** This estimator is used for the "winds behind" and "winds inside" estimates and assumes that winds behind the gust front are perpendicular to the orientation of the gust front. The radial Doppler velocity values v_r within the analysis region are converted to horizontal wind speeds $|V|$ using the relationship:

$$|V| = v_r / \cos \Psi$$

where Ψ is the difference between the radar azimuth and the angle perpendicular to the orientation of the gust front. This calculation is unstable for large Ψ which occurs when the gust front is nearly radially aligned, so Ψ is constrained to a maximum of 60 degrees. The weight for this estimate is a function of the viewing angle, with greatest weight given when the gust front is oriented perpendicular to the radar azimuth.

2. **Optimal estimation.** A linear least-squares technique called optimal estimation (used in the ITWS Terminal Winds algorithm [Cole, 1994]) is used to compute a wind speed and direction from a sample of radial Doppler velocity values together with a background wind estimate for guidance. For "winds behind" and "winds inside" estimates, the gust front propagation velocity is used as the background vector. For the "winds ahead" estimate, gust front characteristics cannot be used to supply a background wind vector and the computation reduces to a traditional least-squares fit of radial velocity assuming a uniform wind model. The calculation produces not only an estimate, but also a covariance error value indicating confidence in the estimate. This technique tends to fail when the angle between the radial and the true wind direction is large. It also tends to fail when there is a wind shear across the sampling region. The covariance error value is translated into a weight value. The weight value is further decreased if the viewing angle is large or if there is significant variation among sample values.

3. **Airport anemometer measurements.** For a gust front that has just crossed the airport, an airport anemometer (such as the LLWAS centerfield anemometer or from ASOS) provides the most direct measurement of the near-surface winds behind the gust front. Likewise, for a gust front that is approaching and is in close proximity to the airport, the anemometer provides a good measure of the ambient winds ahead of the front, which can be used in determining the wind shear hazard. However, representativeness of this measurement decreases with distance from the location where winds are to be estimated. Thus, this estimate is given a high weight when close to the desired wind analysis region and progressively lower weights with increasing distance.

4. **Radar site wind.** The wind velocity at the radar site is estimated using a least-squares fit of the Doppler values within a 2.5 km radius of the radar, assuming a uniform wind field. This estimate is temporally smoothed with prior site wind estimates using a weighted average. As with the airport anemometer estimate, representativeness decreases with increasing distance; the weight given to this estimate is reduced accordingly.

5. **Persistence (history).** The consensus wind estimate from the previous processing interval can be used both as a default value and as a dampening mechanism when averaged with other wind estimates. The weight assigned to the persistence estimate is computed as a fraction of the prior consensus weight, depending on how close the attributes of the previous gust front chain matches the current one (i.e., proximity and propagation direction).

6. **ITWS Terminal Winds algorithm output.** Additional estimates for each of the three analysis regions can be obtained from the surface-layer 2 km resolution gridded output of the ITWS Terminal Winds Algorithm. Wind estimate weights are decreased as the time difference between the Terminal Winds data and the TDWR base data in-

creases. Weights are also adjusted as a function of the corresponding error covariance value that accompanies each Terminal Winds gridded wind point. These data are not currently being incorporated by MIGFA, so (for now) the weights are being set to zero.

4. WIND SHEAR HAZARD ESTIMATION

Some gust fronts can produce hazardous levels of wind shear. Current operational requirements for the gust front product stipulate that a wind shear alert shall be issued whenever a gust front having a ΔV exceeding 15 knots intersects a runway approach or departure corridor. Historically, the length interval over which this quantity has been computed has been 1 km. Once again, MIGFA uses a consensus approach to obtaining this estimate, with varying weights assigned to individual estimates based on situational context. Currently MIGFA computes the ΔV as a weighted average of estimates obtained from three different estimation techniques:

1. **Radial shear map.** The most direct technique, and the one that most closely provides the 1 km change in winds, is to retrieve ΔV values directly from the areas of the radial shear map (DV image) that correspond to the detected frontal position. The estimate is weighted by the variance of the population of individual radial shear values and by the distance of the shear location from the radar site (shear values tend to be less reliable as range increases due to decreasing signal–to–noise ratios).

2. **Vector difference.** With this estimator, the ΔV across the front is computed using previously computed consensus estimates obtained behind and ahead of the front. Figure 5 illustrates the vector geometry. ΔV is computed as the magnitude difference between the winds immediately behind the front (the "inside" winds), V_b, and the vector component of the wind ahead of the front, V_a, that is parallel to V_b (labeled V_a'). This estimator is less likely to give the 1–km change than the radial shear map method, since it is insensitive to the velocity gradient of the front. Figure 6 illustrates this problem with three example radial velocity profiles across a front where the end–to–end vector difference is the same, but the 1 km change in velocity across the frontal zone is quite different.

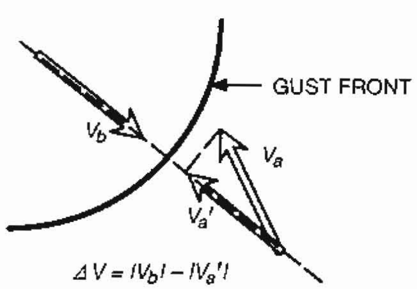

Figure 5. Illustration of vector difference method for computing wind shear hazard (ΔV).

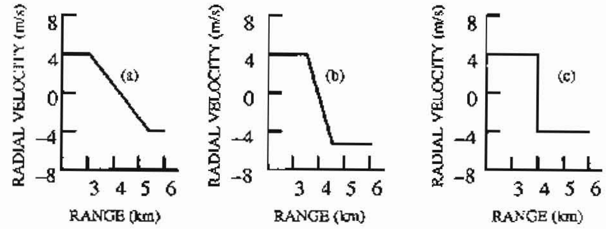

Figure 6. Example radial velocity profiles across three fronts having different cross–front gradients, but the same end–to–end velocity change. The vector difference method would yield a ΔV of 8 m/s for each profile, which is the same as the 1–km change in (c). By contrast, the 1–km ΔV is quite different for cases (a) and (b).

3. **Persistence (history).** The previous ΔV estimate for the gust front is used as a persistence–based estimate of the current ΔV. The estimate is weighted by how closely the location and associated propagation direction of the current gust front analysis segment match those of the previous detection.

5. WIND SHIFT ESTIMATION

On the user's graphical Situation Display, a numbered arrow placed behind the current gust front location denotes the expected wind speed and direction after gust front passage, i.e., the wind shift. Controllers use this information together with the predicted gust front locations to plan runway usage. ATC representatives have stated that for the wind shift product to be operationally useful, the displayed wind shift estimate should indicate what the winds will be at the airport 10 minutes after gust front passage. The implicit reasoning behind this requirement is that a wind shift of duration less than 10 minutes is not worth the delay that might be incurred by reconfiguring the runways. For short–duration wind shifts, controllers would prefer to "wait it out" with the current runway configuration, holding traffic if necessary.

For each detected gust front, MIGFA uses the propagation speed and direction of the front to determine the wind shift analysis region (i.e., the "winds behind" region) that corresponds to "10 minutes" behind the front (as shown in Figure 3). The weighted average consensus of estimators for the "winds behind" region is then used as the wind shift forecast.

6. RESULTS

6.1. Detection Performance

MIGFA has been extensively field tested at a number of different locations over the last four years using ASR–9 WSP (Orlando, FL; Albuquerque NM) and TDWR/ITWS (Orlando, FL; Memphis, TN; Dallas–Ft. Worth, TX) testbed radar systems operated by Lincoln Laboratory. During these live operational field tests, MIGFA provided real–time gust front products to air traffic controllers and user feedback was obtained. Input radar and anemometer data together with algorithm output products were archived for subsequent performance analysis. Results from several different performance assessments have been documented in prior publications [Troxel, 1995; Klingle–Wilson, 1995]. During two recent tests of ITWS (Orlando, 1993 and Dallas, 1995), MIGFA was run concurrently with the production TDWR gust front algorithm (GF88), providing an opportunity for comparing the performance of MIGFA against an existing standard. Performance of both algorithms was assessed by automated scoring of algorithm detections against a truth database generated by visual inspection of each input image processed by the two algorithms.

To generate the truth database, an expert analyst inspected successive Doppler velocity and reflectivity images from the TDWR separately or in rapid sequence as a movie. For each scan image, the analyst entered a list of coordinates marking the gust front end points along with an intermediate sampling of points in between. For categorization of results, the estimated maximum wind shear in the convergence zone was also stored.

An automated scoring procedure, described in detail by Klingle–Wilson [1992] compares computed gust front detections against coordinates contained in the truth database. Briefly, the scoring algorithm connects the sequence of coordinates defining the limits of the gust front and expands the collection of connected line segments into a 5–km wide region that is called a truth box. The scoring program assesses detection performance by two metrics. The first measure is a crude event–based statistic that counts a detection as valid if any part of the detection overlaps any part of a truth box. A detection is counted as false if it falls completely outside of any truth boxes. An overall probability of detection (POD) is computed by dividing the number of successfully detected fronts by the number of fronts identified by the human analyst. The probability of false alarm (PFA) is the number of false detections divided by the total number of detections (both valid and false). A second, more rigorous metric measures detection quality by comparing the length of the front against the length identified by the human analyst. The percent length detected (PLD) is expressed as a ratio of the length detected to the length delimited by the human analyst. The percent of false length detected (PFD) reflects the fraction of total detection length that was not verified by truth.

Tables 1 and 2 compare the automated scoring results categorized by strength for MIGFA and GF88 for the Orlando (MCO) and Dallas (DFW) test sets. Orlando results were computed from a substantial database comprised of 2750 images from 230 hours of data collected on 30 different days during the test period. Dallas results were computed from a more limited data set comprised of 456 images from 35 hours of data on 6 different days. As can be seen from the tables, MIGFA outperformed the current TDWR gust front algorithm at both locations, especially for the weaker gust fronts. MIGFA correctly detected and tracked over 70% of all gust fronts identified by human analysts, compared to a best effort of 40% at DFW for the existing GF88 algorithm. An apparent exception in the 15 knot category of DFWgust fronts is most likely insignificant since this category contained only 11 total images from a single gust front. For this one event, MIGFA was two scans later than GF88 in reporting the gust front.

MIGFA did an even better job of detecting the overall length of gust fronts. For example, at Orlando MIGFA detected 57% of the total length of all gust fronts, representing a five–fold improvement over GF88 performance in this category.

MIGFA's substantial improvement in detection performance over the existing detection algorithm can be understood by considering that the current TDWR algorithm utilizes traditional 1–D processing of radial Doppler velocity convergence signatures [Uyeda, 1986] as its primary means of detection. Without spatial context and additional information from other sources of evidence such as reflectivity thin lines and motion, the GF88 algorithm is at a disadvantage. Some other recent experimental algorithms have attempted to make additional use of thin line recognition [Eilts, 1991], but modest improvements in detection probability have often been accompanied by undesirably high false alarm probabilities. Once again, the traditional 1–D processing methods limit achievable performance gains.

6.2. Wind Shift and Wind Shear Hazard Report Accuracy.

MIGFA wind shift forecasts were compared against LLWAS centerfield anemometer data for 53 gust fronts that were detected by MIGFA and that tracked over the airport during ITWS operational testing at Memphis in 1994 and 1995. Results were obtained by comparing MIGFA wind shift reports generated while the gust front was 10 minutes away from the airport against airport centerfield anemometer measurements taken between seven and 13 minutes after gust front passage over the airport.

Wind shear hazard (ΔV) estimate accuracy was also assessed using a subset of 35 gust fronts from 1994, . Algorithm wind shear hazard reports that were generated while the gust front was impacting the airport were compared against wind shear hazard estimates obtained by visual analysis of TDWR Doppler velocity data in conjunction with centerfield anemometer data.

Table 3 lists mean errors and error standard deviations for the ΔV estimate and for the wind speed and wind direction components of the wind shift forecasts. As can be seen from the table, MIGFA's wind shear and wind shift forecasts are generally consistent with observations. The wind direction component of the wind shift forecasts show the widest discrepancies with a mean error of 22 degrees and a standard deviation of absolute differences of 16 degrees. These numbers are comparable to those reported in earlier studies of the current TDWR gust front algorithm. For example, Hermes [1993] examined 117 gust fronts and reported a mean direction error of 24 degrees and a standard deviation of 18 degrees for the current TDWR algorithm.

Table 1. Performance comparison between the current TDWR gust front algorithm (GF88) and MIGFA for Orlando gust fronts.

ORLANDO (2750 IMAGES)	PROBABILITY OF DETECTION (%) / [PERCENT LENGTH DETECTED]				PROBABILITY OF FALSE ALARM (%) / [PERCENT FALSE LENGTH DETECTED]
ΔV (m/s)	5 – 10	10 – 15	> 15	ALL	
GF88	28 / [10]	65 / [31]	–	31 / [11]	8 / [17]
MIGFA	70 / [57]	84 / [66]	–	71 / [57]	3 / [7]

Table 2. Performance comparison between the current TDWR gust front algorithm (GF88) and MIGFA for Dallas gust fronts.

DALLAS (456 IMAGES)	PROBABILITY OF DETECTION (%) / [PERCENT LENGTH DETECTED]				PROBABILITY OF FALSE ALARM (%) / [PERCENT FALSE LENGTH DETECTED]
ΔV (m/s)	5 – 10	10 – 15	> 15	ALL	
GF88	29 / [18]	83 / [40]	100 / [51]	40 / [27]	10 / [11]
MIGFA	74 / [60]	94 / [68]	94 / [80]	78 / [64]	6 / [19]

One possible source of discrepancy between MIGFA wind shift estimates and "truth" observations is the difference in altitude between the area being sampled by the radar and the point near the ground being measured by the anemometer. When wind direction values obtained by inspection of TDWR Doppler images were compared against corresponding LLWAS centerfield anemometer measurements, a mean difference of 25 degrees and a standard deviation of 31 degrees was obtained. This suggests that some of the discrepancies between MIGFA and LLWAS centerfield wind direction estimates can be attributed to differences between wind measurements obtained by the two sensors. Hermes [1993] cited height differences of as much as 140 m between areas scanned the radar and the region sampled by a ground–based anemometer as a possible factor in observed differences with the current TDWR wind shift algorithm.

Table 3. MIGFA report error for wind shear (ΔV) and wind shift (speed and direction) estimates.

	MEAN ERROR	STD. DEV.
ΔV	1.5 m/s	1.2 m/s
SPEED	1.6 m/s	1.4 m/s
DIRECTION	22.0 deg	16.2 deg

6.3. Limitations of MIGFA Wind Shift Forecasts.

There are a number of problems that can limit MIGFA's ability to produce accurate wind shift forecasts. One problem is that outflow characteristics can vary considerably in the area between the gust front boundary and the wind shift analysis region, making determination of a single representative wind shift estimate difficult. For example, the relatively cold thunderstorm outflow can be thought of as a density current. Laboratory fluid tank modeling and analyses have shown that such density currents can produce so–called "gravity waves" that induce oscillations in the flow [Simpson, 1987]. We have periodically observed these gravity waves behind strong gust fronts, where they produce pronounced short–period fluctuations in wind speed and direction (Figure 7).

Another interesting problem is that of the detached outflow boundary, or horizontal roll [Wakimoto, 1982]. These types of gust fronts continue to propagate, but are no longer continuously fed by the original generating thunderstorm. They often produce a momentary wind shift, followed by a relatively quick return to ambient (pre–gust front) wind conditions. All of this may occur in a relatively small area located between the leading edge of the gust front and the "winds behind" region chosen by MIGFA for the wind shift analysis. When this occurs, MIGFA may actually produce a wind shift vector that points in a direction opposite the propagation direction of the gust front. This is not necessarily incorrect, since a wind shift arrow pointing in the same direction as the current ambient airport winds would suggest to ATC that any wind shift associated with the incoming gust front will not persist long enough to warrant changing a runway configuration.

TDWR data quality has been a significant cause of MIGFA detection and wind estimation failure. Perhaps the most difficult data quality problem for MIGFA is that of velocity data errors introduced by the TDWR velocity dealiasing algorithm. The velocity dealiasing algorithm attempts to resolve Doppler velocity measurement ambiguities resulting from wind speeds that exceed the radar's unambiguous velocity range by "unfolding" the ambiguous measurements into the correct velocity interval [Sykes, 1991; Wieler, 1991]. When dealiasing errors occur, artificial velocity convergence boundaries are sometimes generated that can mimic strong gust front convergence signatures and could cause false detections. For MIGFA, we have developed a special detector that examines local distributions of velocities

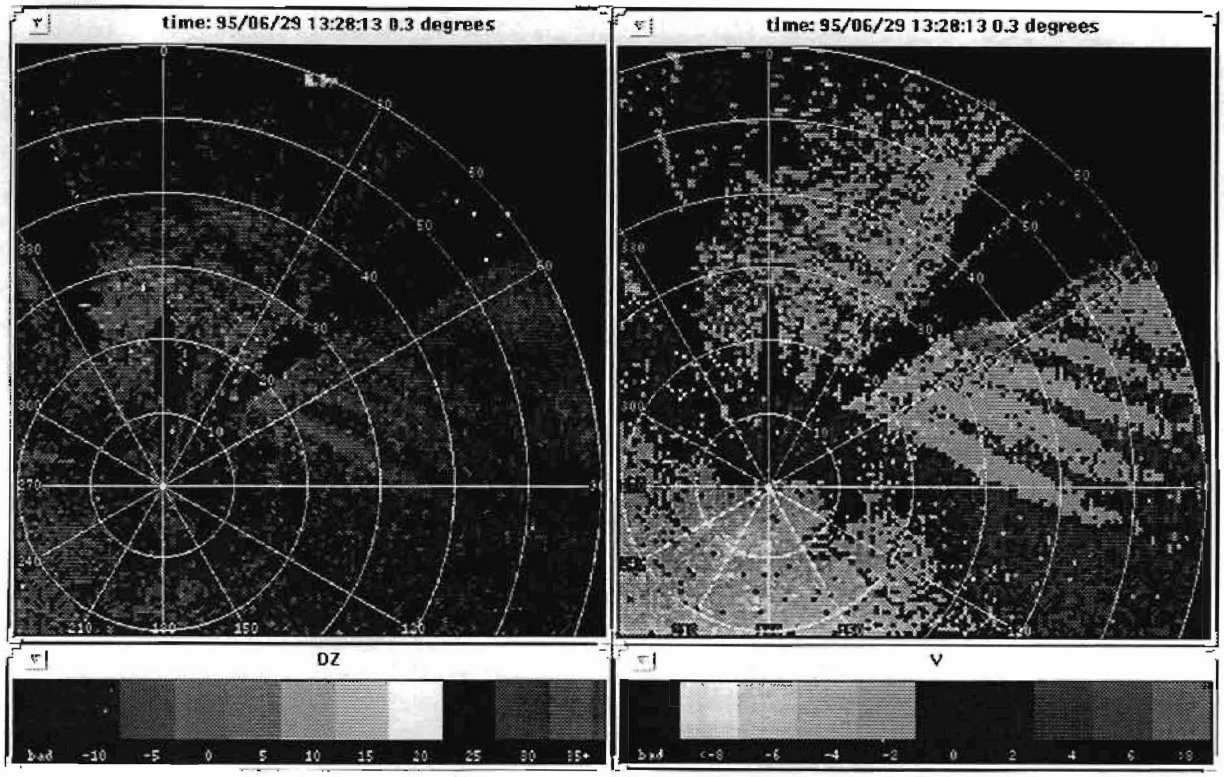

Figure 7. Gravity waves behind a gust front seen in TDWR reflectivity (left) and Doppler velocity (right) imagery. Reflectivity scale (DZ) is in dBZ and velocity scale (V) is in m/s with lighter shades indicating winds directed toward the radar, and darker shades indicating winds directed away from the radar. Range rings are in km. The gust front is oriented from WNW to ESE and the nearest edge is at approximately 15 km from the radar. Note in particular, the oscillations in the Doppler velocity imagery with a period of approximately 6.5 km (10 minutes).

and recognizes the sharp Nyquist–interval jump in radial velocity that is characteristic of these dealiasing errors. Strong negative interest is generated along these error boundaries. The negative interest is then used to suppress positive interest that would be generated by MIGFA's convergence detectors.

There is another type of velocity dealiasing failure that is more problematic for wind shift estimation. The TDWR dealiasing algorithm utilizes a windfield model for guidance in unfolding the velocities into the correct velocity Nyquist interval. We have observed numerous instances where the windfield model appears to misinterpret the shear across some gust fronts as aliasing, especially if the gust front is propagating into a sparse data region. This causes the dealiasing algorithm to improperly unfold a substantial area of the velocity field behind the front. Figure 8 shows an example of this. Such inappropriately "corrected" velocity data can lead to wind shift estimate errors if these regions are subsequently processed with MIGFA's wind shift estimators. The robustness of MIGFA's consensus method of wind estimation helps to limit, but not eliminate, the impact of these bad velocity values on the final results. Nonetheless, we are currently working on techniques to identify these error regions (not just the error region boundaries) so that they will not be incorrectly processed during wind shift estimation.

Other causes of missed wind shift forecasts include rapidly evolving gust fronts, complex wind fields due to interactions with other outflows from nearby storms, and fronts that dissipate before reaching the airport.

7. SUMMARY AND FUTURE WORK

Automated gust front detection and tracking, together with associated wind shear warnings and wind shift forecasts, serve important traffic safety and route planning needs for ATC. Previous reports by the authors have focussed primarily on methods for detecting and tracking gust fronts, with primary attention given to the signal processing and machine intelligence techniques used. By contrast, this report provides a more in–depth discussion of the additional wind shift and wind shear processing tasks required to complete the gust front product.

After providing a brief review of the detection algorithm, we first presented an update on the latest MIGFA detection capabilities using data obtained from recent field tests conducted in Orlando, FL and Dallas, TX. During these real–time tests, MIGFA was run side–by–side with the existing TDWR gust front algorithm and detection performance was assessed. At both locations, MIGFA substantially outperformed the existing TDWR gust front algorithm (GF88), not only in terms of the number of fronts detected, but also in terms of the total lengths of the detected gust fronts. As a result of this demonstrated improve-

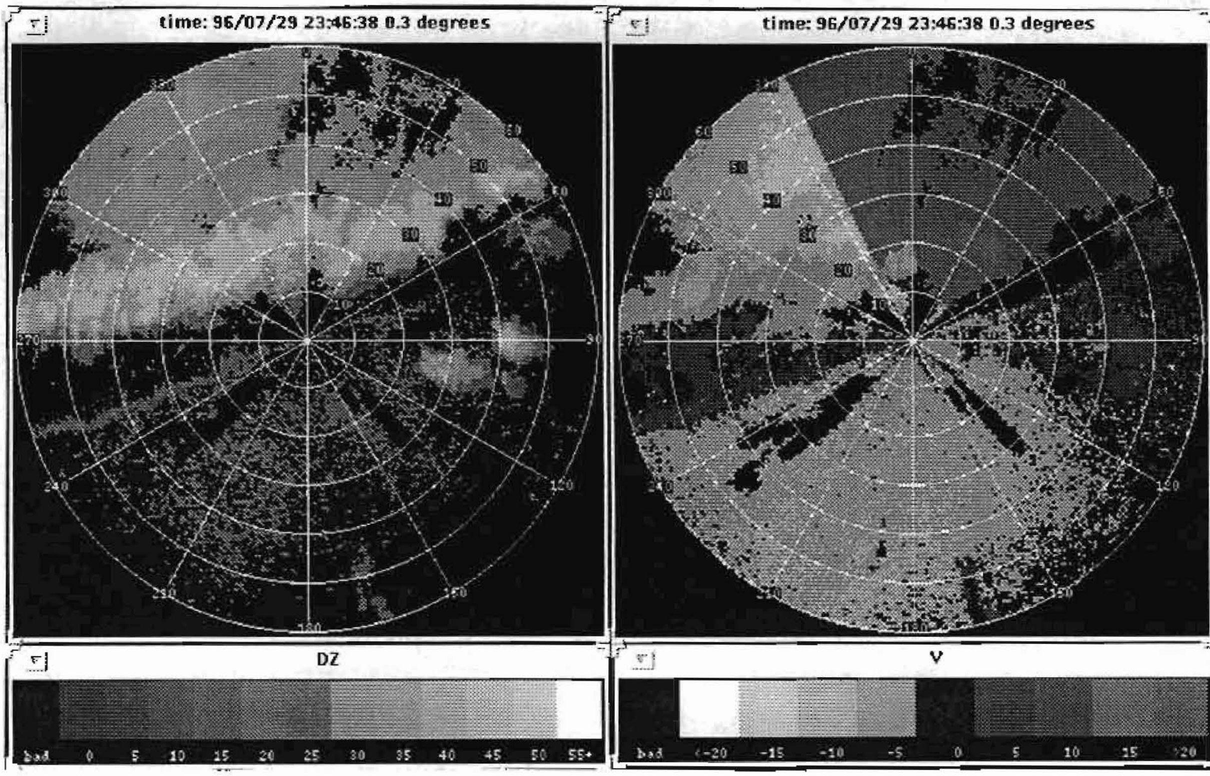

Figure 8. Example of TDWR velocity dealiasing errors contaminating the velocity field behind a gust front. Part of the gust front can be seen in the reflectivity image (left) as a 5 dBZ thin line extending WSW from the radar and 15 km ahead of the intense line of thunderstorms. In the corresponding velocity image (right), erroneous velocity values fill a sector extending from approximately 335 degrees to 60 degrees azimuth. These values are incorrectly represented as outbound velocities (dark grays). Reflectivity scale (DZ) is in dBZ and velocity scale (V) is in m/s with lighter shades indicating winds directed toward the radar, and darker shades indicating winds directed away from the radar. Range rings are in km.

ment, work is currently underway to equip existing TDWRs with the additional hardware computational capability needed (via dedicated "outboard" workstations) to use MIGFA as an upgrade replacement for the current TDWR gust front product generator.

The bulk of this report focussed on details of MIGFA's wind shift and wind shear estimation techniques. Rather than rely on a single wind estimation technique, MIGFA performs wind analyses in regions 10 minutes behind, immediately behind, and ahead of the front using a variety of wind estimation techniques including optimal estimation, least squares fit of Doppler values to a uniform wind model, direct anemometer measurements, perpendicular wind model, and persistence (history). Consensus estimates for each of the three windfield analysis regions are formed by weighting and averaging the individual estimates using rules that account for situational context. Consensus estimates for the region 10 minutes behind the front are used for the wind shift forecasts. These were compared against LLWAS centerfield anemometer measurements and were shown to be accurate well within operational requirements.

A number of issues and difficulties pertaining to making operationally useful wind shift forecasts were discussed. Winds behind many gust fronts can often exhibit considerable variability over relatively short time and distance scales, making determination of a single representative wind shift estimate difficult. TDWR data quality, particularly where velocity dealiasing was incorrectly applied, was shown to be a considerable factor affecting reliability of MIGFA wind shear and wind shift estimates. MIGFA currently has specific algorithm logic to recognize artificial convergence boundaries occasionally produced by these dealiasing errors. Additional techniques are being developed to limit corruption of MIGFA wind shift estimates from these data quality problems.

As a near-term algorithm enhancement, we plan to incorporate 2-km gridded wind analyses available from the ITWS Terminal Winds algorithm [Cole, 1994]. These gridded wind data, computed by combining data from a national numerical weather-prediction model (RUC) with observations from ground stations, aircraft reports, and Doppler weather radars, would serve as an additional "estimator" to help refine MIGFA's wind shift and wind shear reports. This effort will need to be coordinated with Terminal Winds algorithm developers. The Terminal Winds algorithm needs feedback from MIGFA regarding locations of gust fronts so that wind estimates are not spatially smoothed across actual windfield discontinuities produced by gust fronts.

8. REFERENCES

Cole, R.E. and F.W. Wilson, 1994: "The Integrated Terminal Weather System terminal winds product," *Lincoln Laboratory Journal*, Vol. 7, No. 2, 475–501, 1994.

Delanoy, R. L., J. G. Verly, and D. E. Dudgeon, 1992: "Functional templates and their application to 3–D object recognition," *Proceedings of the 1992 International Conference of Acoustics, Speech, and Signal Processing*, San Francisco, CA, March 23–26, 1992.

Delanoy, R. L., and S. W. Troxel, 1993a: "Machine intelligent gust front detection," *Lincoln Laboratory Journal*, Vol. 6, No. 1, 187–211, 1993.

Delanoy, R. L., J. G. Verly, and D. E. Dudgeon, 1993b: "Pixel–level fusion using interest images," *Technical Report TR–979*, MIT Lincoln Laboratory, Lexington, MA, May 1993.

Eilts, M., S. Olson, G. Stumpf, L. Hermes, A. Abrevaya, J. Culbert, K. Thomas, K. Hondl, and D. Klingle–Wilson, 1991: "An improved gust front detection algorithm for the TDWR," *Proc. 4th Intl. Conf. on the Aviation Weather System*, Paris, June 1991, p. J37.

Hermes, L., A. Witt, S. Smith, D. Klingle–Wilson, D. Morris, G. Stumpf, and M. Eilts, 1993: "The gust front detection and wind shift algorithms for the Terminal Doppler Weather Radar system," *J. Atmos. Oceanic Tech.*, Vol. 10, No. 5, 693–709, October, 1993.

Klingle–Wilson, D. L., M. F. Donovan, S. H. Olson, and F. W. Wilson, 1992: "A comparison of the performance of two gust front detection algorithms using a length–based scoring technique," *Project Report ATC–185*, MIT Lincoln Laboratory, Lexington, MA, May 1992.

Klingle–Wilson, D.L., editor, 1995: "Integrated Terminal Weather System (ITWS) Demonstration and Validation Operational Test and Evaluation," *Project Report ATC–234*, MIT Lincoln Laboratory, Lexington, MA, April, 1995

Lincoln Laboratory, 1995: "Integrated Terminal Weather System (ITWS) Algorithm Description – Chapter 6: Machine Intelligent Gust Front Algorithm," *Report No. DOT/FAA/ND–95/11*, Vol. 1 of 3, October, 1995.

Simpson, J.E. 1987: *Gravity Currents in the Environment and the Laboratory*, published by Ellis Horwood Limited.

Sykes, T.D., and B.H. Stevens, 1991: TDWR Velocity Dealiasing Algorithm in Operation, Preprints, *25th Intl. Conf. on Radar Meteorology, Paris, France*, Amer. Meteor. Soc., Boston, MA., 350–353.

Troxel, S., and R. L. Delanoy, 1994: "Machine intelligent approach to automated gust front detection for Doppler weather radars", *SPIE Proceedings – Sensing, Imaging, and Vision for Control and Guidance of Aerospace Vehicles*, Vol. 2220, 182–192, Orlando, FL, April 4–5, 1994.

Troxel, S.W., and R.L. Delanoy, 1995: Machine intelligent gust front detection for the Integrated Terminal Weather System, *Sixth Conference on Aviation Weather Systems*, Dallas, Texas, Amer. Meteor. Soc., 378–383

Uyeda, H., and D. S. Zrnic', 1986: "Automated detection of gust fronts," J. Atmos. Oceanic Tech. 3, 36, 1986.

Verly, J. G., R. L. Delanoy, and D. E. Dudgeon, 1989: "Machine intelligence technology for automatic target recognition," *Lincoln Laboratory Journal*, Vol. 2, No. 2, 277–311, 1989.

Wakimoto, R.M., 1982: The life cycle of thunderstorm gust fronts. *Monthly Weather Review, 110: 1060–1082.*

Wieler, J.G., 1991: TDWR velocity dealiasing. Preprints. *25th International Conference on Radar Meteorology, Paris, France*, Amer. Meteor. Soc., Boston, MA., 347–349